Real-Time Monitoring of the Interactions of Two-Stranded *de Novo* Designed Coiled-Coils: Effect of Chain Length on the Kinetic and Thermodynamic Constants of Binding†

Gregory De Crescenzo,[#] Jennifer R. Litowski,[§,‡] Robert S. Hodges,[§,‡] and Maureen D. O'Connor-McCourt*,[#]

Cell Surface Receptor Group, Health Sector, Biotechnology Research Institute, National Research Council (Canada), 6100, Royalmount Avenue, Montreal, Quebec, Canada H4P 2R2, Department of Biochemistry, University of Alberta, Edmonton, Alberta, Canada T6G 2H7, and Department of Biochemistry and Molecular Genetics, University of Colorado Health Sciences Center, 4200 E. 9th Avenue, Denver, Colorado 80262

Received September 13, 2002; Revised Manuscript Received December 18, 2002

ABSTRACT: We have de novo designed a heterodimeric coiled-coil formed by two peptides as a capture/delivery system that can be used in applications such as affinity tag purification, immobilization in biosensors, etc. The two strands are designated as K coil (KVSALKE heptad sequence) and E coil (EVSALEK heptad sequence), where positively charged or negatively charged residues occupy positions e and g of the heptad repeat. In this study, for each E coil or K coil, three peptides were synthesized with lengths varying from three to five heptads. The effect of the chain length of each partner upon the kinetic and thermodynamic constants of interaction were determined using a surface plasmon resonance-based biosensor. Global fitting of the interactions revealed that the E5 coil interacted with the K5 coil according to a simple binding model. All the other interactions involving shorter coils were better described by a more complex kinetic model involving a rate-limiting reorganization of the coiled-coil structure. The affinities of these de novo designed coiled-coil interactions were found to range from 60 pM (E5/K5) to 30 μM (E3/K3). From these K_d values, we were able to determine the free energy contribution of each heptad, depending on its relative position within the coiled-coils. We found that the free energy contribution of a heptad occupying a central position was 3-fold higher than that of a heptad at either end of the coiled-coil. The wide range of stabilities and affinities for the E/K coil system provides considerable flexibility for protein engineering and biotechnological applications.

The α-helical coiled-coil is an oligomerization domain that is naturally present in a wide variety of proteins such as transcription factors, cytoskeletal proteins, motor proteins, and viral fusion proteins (*1*−*3*). The structural properties of coiled-coils have been extensively characterized from numerous high-resolution crystal and NMR structures (*3*−*5*). The formation of coiled-coils requires the wrapping of two or more amphipathic α-helices around each other in a left-handed supercoil fashion; the helices may be aligned in either a parallel or antiparallel manner. The α-helices composing the coiled-coil structure are defined by a heptad repeat (denoted abcdefg) in which hydrophobic residues occupy the positions a and d and pack in a characteristic "knobs-into-holes" manner (*6*), forming the hydrophobic core (Figure 1). Many studies (*1*, *7*−*12*) emphasized the role of charged residues (typically in the e and g positions) in controlling the specificity of oligomerization and opened up the way to the de novo design of heterodimeric coiled-coils (*13*−*17*). Their relatively small size, in addition to their well-defined structure, make coiled-coils a very attractive system for protein engineering and biotechnological applications (*5*, *18*) such as the construction of miniaturized antibodies, the control of signaling protein domain oligomerization, and the specific targeting of GFP to cytoskeletal proteins (see ref 4 for review).

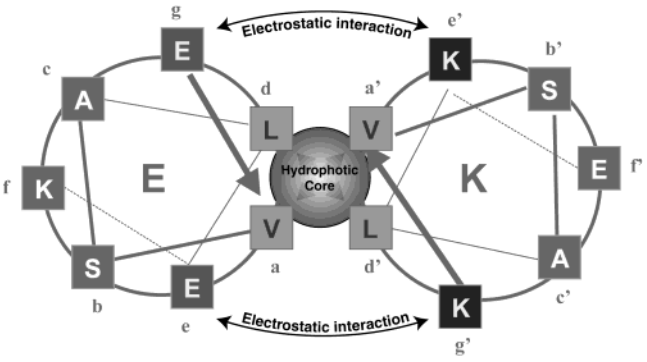

FIGURE 1: Helical wheel representation of the E/K coiled-coil heterodimer, in which one heptad is viewed in cross-section. The interhelical hydrophobic interactions are indicated by the circle. The arrows denote the pairs of interchain electrostatic interactions on each side of the hydrophobic core. Peptide nomenclature is described in Table 1.

† This work was supported by the Protein Engineering Network of Centres of Excellence (PENCE), Sensium Technologies, Inc., the Canadian Institutes of Health Research group in Protein Structure and Function, and the University of Colorado Health Sciences Center. G.D.C. is supported by PENCE, and J.R.L. is supported by an Izaak Walton Killam doctoral scholarship and an Alberta Heritage Foundation for Medical Research Incentive Award.

* To whom correspondence should be addressed. Tel: 514-496-6382. Fax: 514-496-5143. E-mail: maureen.o'connor@nrc.ca.

[#] National Research Council (Canada).

[§] University of Alberta.

[‡] University of Colorado.

10.1021/bi0268450 CCC: $25.00
Published on Web 01/25/2003

We have designed a heterodimeric coiled-coil system formed by two peptides (designated the E coil and K coil) (*19*, *20*) and have shown that this heterodimerization motif is promising not only as a protein expression and purification tag (*21*), but also as a universal dimerization domain for biosensor applications (*22*). The stability and affinity of this E/K system have been successfully modified by varying the α-helical propensity (serine vs alanine), the hydrophobicity of residues in the coiled-coil core (valine vs isoleucine), and the chain length (three to five heptads, or 21 to 35 residues) (*23*, *24*).

In the present paper, we have systematically determined the effect of varying the chain length of each coil, not only upon their affinity, but also upon their kinetics of interaction. To do so, we used a surface plasmon resonance (SPR)-based biosensor, the BIACORE, which allows the real-time monitoring of the interaction between an interactant immobilized at the biosensor surface and a binding partner which is in solution. This technique was shown to be appropriate for peptide interaction studies (*25*).

Both length-matched (i.e., both coils in the dimer having the same length) and mismatched pairs were studied. This approach allowed us to determine the contribution of each heptad, depending on its relative position within the coiled-coil, to the stability of the coiled-coil. Our results showed that it is possible to modulate the affinity of one coil (e.g., E coil composed of five heptads) for its K coil partner by varying the length of the latter from three to five heptads. This characteristic makes the E/K system attractive for a broad range of applications. That is, a single protein/E coil fusion could be used in a variety of applications that require different coiled-coil affinities by using partner K coil peptides of different lengths.

EXPERIMENTAL PROCEDURES

Equipment and Reagents. All the SPR experiments were performed on an upgraded BIACORE 1000. The amine coupling kit containing NHS[1] and EDC, PDEA and PIONEER sensor chips B1 were purchased from BIACORE Inc.

Peptide Synthesis and Purification. The peptides were synthesized by standard *tert*-butyloxycarbonyl (t-Boc) solid-phase techniques developed by Merrifield (*26*) on an Applied Biosystems Peptide Synthesizer model 430A (Foster City, CA), using MBHA resin (0.74 mmol of NH_2/g of resin) (Bachem, Torrance, CA) on a 0.5 mmol scale. The synthesis methodology is similar to that described by Sereda et al. (*27*), except that activation and coupling were performed in situ and described as follows. A 4-fold molar excess of amino acid (2 mmol) was dissolved in DMF and activated with slightly less than equimolar amounts of HBTU and HOBt, and a 5-fold molar excess of DIEA. The side-chain protecting groups were 2-chlorobenzyloxycarbonyl (ClZ) for lysine, *O*-benzyl for glutamic acid, benzyl for serine, and 4-methylbenzyl for cysteine. A common core was synthesized to 21 residues length on a 0.5 mmol scale, at which point the resin was split into three parts and the three related peptides (i.e., K3, K4, and K5) were continued on a 0.1 mmol scale. The peptides were cleaved from the resin by reaction with hydrogen fluoride (20 mL/g resin) containing 10% anisole and 2% 1,2-ethanedithiol for 1.5 h at −5 °C. The resin was washed with diethyl ether to remove the organic scavengers. The peptides were extracted from the resin with glacial acetic acid and the extract was lyophilized.

Crude peptides were purified by reversed-phase chromatography, using a semipreparative Zorbax 300SB-C8 column (250 × 9.4 mm i.d., 5-μm particle size, 300-Å pore size) from Agilent Technologies (Englewood, CO). The following conditions were used: a linear AB gradient of 1% CH_3CN/min from 0 to 10% CH_3CN, followed by a gradient of 0.2% CH_3CN/min, where eluent A was 0.05% aqueous TFA (v/v) and eluent B was 0.05% TFA in CH_3CN. The flow rate was 2 mL/min. The peptides were purified at room temperature, except for VSAL E4 and E5, which were purified at 70 °C to prevent aggregation and improve separation and peak shape. The homogeneity of the purified peptides was verified by analytical reversed-phase HPLC, amino acid analysis, and mass spectrometry.

Analytical reversed-phase runs were performed on a Zorbax 300SB-C8 column (150 × 4.6 mm i.d., 5-μm particle size, 300-Å pore size) or a narrow bore Zorbax 300SB−C8 column (150 × 2.1 mm i.d., 5-μm particle size, 300-Å pore size) from Agilent Technologies (Englewood, CO).

Electrospray mass spectrometry was carried out on a VG Quattro triple quadrupole mass spectrometer from VG BioTech (Altrincham, UK). For direct injections, 10 μL of the sample was injected, the solvent used was 0.1% formic acid in 50% aqueous CH_3CN, and the flow-rate was 50 μL/min. The resulting spectra were scanned from 500 to 1500 Da.

Concentrations were determined by amino acid analysis. Peptides were hydrolyzed in 6 N HCl containing 0.1% (v/v) phenol at 155 °C for 1 h in sealed, evacuated tubes. Amino acid analyses were performed on a Beckman model 6300 amino acid analyzer (Beckman, San Ramon, CA).

SPR Experiments. (a) Immobilization of K coils on Sensor Chips. The different length K coil peptides, which contain N-terminal Cys−Gly−Gly extensions, were immobilized on the surfaces of PIONEER B1 sensor chips using the standard ligand thiol coupling procedure. Surface carboxylic acid groups were activated by the injection of 25 μL of a mixture containing 0.05 M NHS and 0.2 M EDC, yielding the NHS ester. The ester was reacted with the free amine of PDEA (30 μL of 80 mM PDEA in 100 mM boric acid, pH 8.5), a coupling reagent that contains a free amine and a reactive disulfide bond, to yield an active disulfide attached to the dextran via an amide linkage. The K coil was then injected (the free thiol of the N-terminal cysteine undergoes disulfide exchange with the active thiol on the dextran surface), resulting in the peptide being linked to the dextran via a disulfide bond. Specifically, 100 nM K coil freshly dissolved in 10 mM acetic acid, pH 4.0 was injected under manual control until the desired amount of peptide was coupled (50

[1] Abbreviations: CD: circular dichroism; ClZ: 2-chlorobenzyloxycarbonyl; DIEA: *N*,*N*-diisopropylethylamine; EDC: *N*-ethyl-*N*′-(3-dimethylaminopropyl) carbodiimide hydrochloride; EDTA: disodium ethylenediaminetetraacetate; GdnHCl: guanidine hydrochloride; HBTU: 2-(1H-benzotriazole-1-yl)-1,1,3,3-tetramethyluronium hexafluorophosphate; HOBt: *N*-hydroxybenzotriazole; Hepes: *N*-(2-hydroxyethyl)-piperazine-*N*′-2-ethane-sulfonic acid; HBS: Hepes buffered saline; IL-2: interleukine-2; IL-2R: interleukine-2 receptor; MBHA: 4-methylbenzhydrylamine; NHS: *N*-hydroxysuccinimide; PDEA: 2-(2-pyridinyldithio)ethaneamine hydrochloride; RU: resonance unit; SPR: surface plasmon resonance; TFA: trifluoroacetic acid.

to 120 RUs, depending on the individual K coil). Finally, freshly prepared 0.05 M L-cysteine (35 μL, in 0.1 M sodium formate, 1 M NaCl, pH 4.3) was injected to block any remaining activated sites on the sensor chip surface. Control surfaces were prepared similarly, except that running buffer (10 μL) was injected instead of K coil. All steps in the immobilization process were carried out at a flow rate of 5 μL/min.

(b) Kinetic Assays on the BIACORE. All the kinetic experiments were carried out at 25 °C at a flow rate of 100 μL/min, with the exception of E3 and K3, for which the flow rate was 5 μL/min. The running buffer was HBS: 20 mM Hepes, 150 mM NaCl, 3.4 mM EDTA, and 0.05% Tween 20 (pH 7.4). The E coils were dialyzed against the running buffer (which was also used for all dilutions), to minimize changes in bulk refractive index upon sample injection. During the wash-on phase, different concentrations of E coil solutions were injected over a control surface and the various K coil surfaces for 120 s. This was followed by a 360 s wash-off period, during which running buffer flowed over the surface. Regeneration of the sensor chip was accomplished by two pulses of 5 M GdnHCl (15 s each), followed by an EXTRACLEAN and a RINSE procedure, as described in the BIACORE manual, to eliminate all traces of GdnHCl. Duplicate injections of each concentration of E coil were performed in a random order.

(c) Data Preparation and Analysis. Sensorgrams (curves from the wash-on and wash-off phases) were prepared and globally fit using the SP*Revolution* software package freely available on the Internet at the following address: http://www.bri.nrc.ca/csrg/equip.htm#BIACORE. The data were prepared by the method of "double referencing", as described by Rich and Myszka (*25*). Briefly, each concentration of a particular E coil was injected over both the K coil-derivatized surface and the control surface; the control surface sensorgram was subtracted from the K coil sensorgram. In addition, the running buffer was injected over both the K coil-derivatized and the control surfaces. Subtraction of these sensorgrams yielded the buffer blank. Finally, the buffer blank curve was subtracted from the control surface-corrected K coil curves. The resulting data was then converted to concentration units using the molecular weight of the injected species, the equivalence of 1000 RU per 1 ng/mm^2 and a matrix thickness of 100 nm. Each data set, which consists of sensorgrams corresponding to injections of different analyte concentrations over the same surface, was then analyzed using several kinetic models that are available in the SP*Revolution* software package (*28*) and have been described elsewhere (*29*, *30*). A schematic representation of the different kinetic models is shown in Figure 2.

(d) Mathematical Modeling and Parameter Estimation. In SP*Revolution*, the various kinetic models were transposed into differential equations that were solved numerically using an adaptive step-size Runge−Kutta method (*31*) with a nonlinear regression program using Marquardt's algorithm (*32*) to estimate the values of the constants from experimental data. For each model, the kinetic parameters, as well as the quantity of active ligand immobilized on the matrix, were considered as global parameters for a given set of curves. Moreover, two local parameters were added for each curve to take into account the refractive index changes at the beginning of the wash-on and wash-off phases. An evaluation

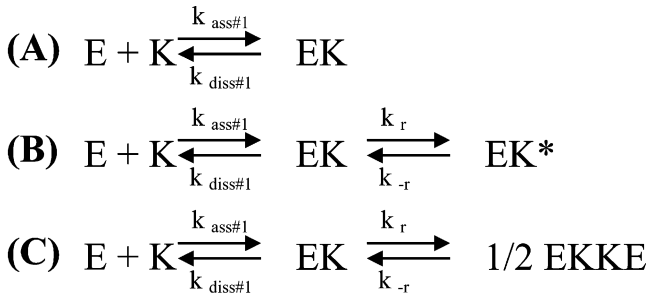

FIGURE 2: Schematic representation of the different kinetic models used to globally fit the E/K interactions. For all models, E and K represent the monomeric forms of the E coil and K coil and EK depicts the coiled-coil complex. (A) Simple Langmuirian interaction. (B) The EK complex undergoes a conformational change (rearrangement) to give EK* (rearranged EK). (C) The E/K complex dimerizes to form tetrameric coiled-coil (EKKE) following the initial monomer-to-dimer step. The kinetic and thermodynamic constant nomenclature is consistent with the one used in the text. For the conformational change model, K_d is defined as the thermodynamic constant related to the first step; $K_d = k_{diss\#1}/k_{ass\#1}$ (M). K_r corresponds to the thermodynamic constant related to the second step; $K_r = k_{-r}/k_r$ (no unit). The apparent K_d (K_{dapp}) of the interaction corresponding to ([E] × [K])/([EK] + [EK*]) at equilibrium is equal to $(K_d^{-1} \times (1 + K_r^{-1}))^{-1}$.

of the quality of the fit for the various kinetic models was done as described elsewhere (*30*) by calculating three statistical values: the standard deviation of the residuals (S.D.), the "+ or − signs" statistic (Z1) and the "Run up and down" statistic (Z2) (*33*).

RESULTS

Peptide Design. We have designed a heterodimeric coiled-coil (Figure 1 and Table 1), based on principles revealed by more than 15 years of investigation (*13*, *16*, *17*, *22*). The primary stabilizing interactions are the hydrophobic interactions in the core (*34*, *37*), electrostatic attractions across the interface (*5*, *7*, *9*, *16*), and helical propensity (*16*, *38*−*41*). Valine and leucine were chosen for positions a and d, as they are known to form a highly stable hydrophobic core (*35*, *36*, *42*, *43*). We have used electrostatic interactions at positions e and g to control specificity for heterodimer versus homodimer formation, an approach successfully exploited in both natural and de novo sequences (*10*−*13*, *16*−*17*, *22*) One strand of the coiled-coil, the E coil, has glutamic acid (which is preferable to aspartic acid because of its higher helical propensity) at all e and g positions, while the complementary K coil has lysine at all e and g positions (Figure 1). In this way, the two homodimers are destabilized by electrostatic repulsions and the E/K heterodimer is stabilized by electrostatic attractions. Serine was placed at position b to increase solubility. Although serine has a low helical propensity, it is the smallest polar, uncharged residue that can increase solubility while minimally interacting with the other side-chains. To compensate, position c was occupied with alanine, the amino acid residue with the highest helical propensity (*16*, *38*−*41*). Although nominally a hydrophobe, alanine has the smallest side-chain, which should discourage aggregation. The K coils have an N-terminal Cys−Gly−Gly extension, which allows them to be immobilized to the BIACORE chip surface via a disulfide-bridge.

Versions of each peptide were synthesized that were three, four, or five heptads long (equivalent to 21, 28, or 35

Table 1: Peptide Sequences and Nomenclature

Name[a]	Sequence[b]
	gabcdefgabcdefgabcdef
E3	Ac-EVSALEKEVSALEKEVSALEK-NH_2
E4	Ac-EVSALEKEVSALEKEVSALEKEVSALEK-NH_2
E5	Ac-EVSALEKEVSALEKEVSALEKEVSALEKEVSALEK-NH_2
K3	Ac-CGGKVSALKEKVSALKEKVSALKE-NH_2
K4	Ac-CGGKVSALKEKVSALKEKVSALKEKVSALKE-NH_2
K5	Ac-CGGKVSALKEKVSALKEKVSALKEKVSALKEKVSALKE-NH_2

[a] E and K denote peptides in which the e and g positions are occupied by glutamic acid or lysine, respectively. The number describes the peptide length in number of heptads. [b] The sequences are written in the one letter amino acid code. Ac represents an N^{α}-acetyl group. NH_2 represents a C^{α}-amide group. Positions a and d of the heptad repeat are underlined and form the hydrophobic core of the coiled-coil.

residues). This is reflected in the nomenclature (Table 1) in which E and K refer to the identity of the residues at positions e and g, and the number refers to the number of heptads in the peptide chain. For example, E3 is the three-heptad peptide with glutamic acid at all e and g positions. E4/K4 denotes the heterodimeric coiled-coil formed by the interaction of the E4 and K4 peptides.

Optimization of the BIACORE Experiments. To monitor binding in real-time between E and K coils of different lengths, and hence to be able to determine not only the thermodynamic but also the kinetic constants depicting the interactions, we chose to use a surface plasmon resonance (SPR)-based biosensor, the BIACORE. In a classical BIACORE experiment, one of the binding partners is immobilized in the matrix of a sensor chip surface and the other interactant is injected over that sensor chip surface. As the injection is proceeding, a mass accumulation of the analyte (the injected species in BIACORE terminology), as it binds to the ligand (the immobilized species), causes an increase in the refractive index of the interfacing medium at the surface and this is recorded in arbitrary resonance units (RU). This signal is proportional to the mass accumulation of the analyte. This corresponds to the wash-on phase of the experiment. The analyte solution is then replaced by buffer and dissociation of the surface complexes is recorded (the wash-off phase). If complexes still remain in the matrix at the end of the wash-off phase, their elution can be achieved by injecting a regeneration solution that promotes dissociation of the complexes without damaging the ligand. This series of steps constitutes a sensorgram. By repeating the experiment with a series of different analyte concentrations, a set of sensorgrams is recorded. Since the data are recorded in real-time, it is possible to derive kinetic parameters from the analysis of the set of curves. This experimental approach, in combination with numerical integration methods that globally fit all the sensorgrams in a set at the same time, has been shown to be reliable for discriminating between different mechanisms of binding and for determining the values of the related kinetic constants (*30*, *44*, *45*). However, artifacts that could bias the analysis must be eliminated prior to the determination of the kinetics of binding (*25*). The first step in our study was to test for and eliminate artifacts that could result from nonoptimal experimental design.

Most of the BIACORE biosensor artifacts identified to date are related to surface effects since one of the interactants must be immobilized to the sensor surface. The most obvious artifact is surface ligand heterogeneity; this can occur when more than one coupling site is present in the ligand molecule (*46*−*48*). The de novo designed E and K coils are relatively small peptides whose molecular weights vary from 2300 to 4100 Da, each of them containing multiple carboxyl and amino groups. Thus, carboxyl and amine coupling strategies cannot be used. The strategy chosen for this study was to add a three-residue extension (Cys−Gly−Gly) to the amino terminus of the coils. This linker enabled us to couple the K coils to the surface using thiol coupling chemistry and hence to generate homogeneous, oriented surfaces. Another surface-related artifact, referred to as the "parking" or "crowding" problem, corresponds to the masking of ligand molecules by previously formed complexes. This phenomenon, first described by O'Shannesy (*48*), is particularly critical when the molecular weight of the analyte is large compared to the ligand. Since the two binding partners have almost the same size and are relatively small, it is unlikely that this "parking problem" would occur during our experiments. However, to reduce or eliminate this and other artifacts such as mass transport limitation and rebinding (*49*), we coupled the minimal quantity of K coils required to detect the interactions with an acceptable signal-to-noise level (between 50 and 150 RUs of K coil). The flow rate was also set to the maximum possible (100 μL/min) for all experiments (except for the E3/K3 interaction) not only to minimize mass transport and rebinding artifacts, but also to promote faster changes between running and sample buffer (*25*). Nonspecific interactions were minimal as assessed by performing injections over a control surface (no K coil immobilized) and were subtracted out by applying the "double referencing" procedure which Myszka (*25*, *50*) has suggested to be critical in the analysis of low molecular weight analytes.

Characterization of the E/K Interactions. We applied the procedure described above to study the interactions between coils of different chain lengths. The sensorgram data set from the binding of E5 and K5 (Figure 3) was globally fit to a simple langmuirian model of interaction. This is a model in which the unfolded monomeric E5 and K5 peptides interact to form a fully folded dimeric coiled-coil in a single step, without discernible intermediates (Figure 2). The high quality of the fit can be judged visually by examining the distribution of the residuals (the difference between calculated and experimental points, Figure 3B). The on-rate determined by

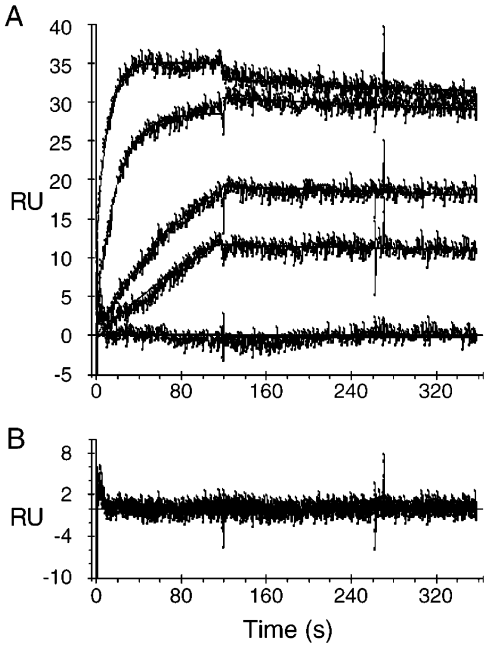

FIGURE 3: Global analysis of the E5 interaction with K5. (A) Global fit of the E5 interaction with K5 using the simple binding model: Different concentrations of E5 ranging from 100 to 5 nM were injected over approximately 50 RUs of immobilized K5 and over a control dextran surface. The points correspond to the RUs obtained after double referencing. The solid lines represent the fit when integrating the curves simultaneously using a simple Langmuirian model. (B) Residuals from A.

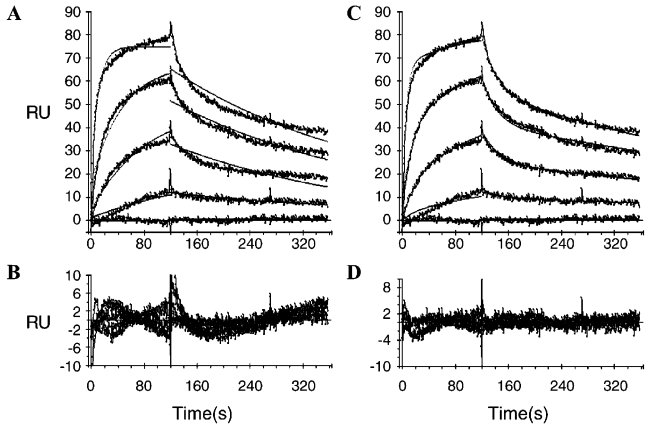

FIGURE 4: Global analysis of the E4 interaction with K4. (A) Global fit of the E4 interaction with K4 when using the simple binding model: Different concentrations of E4 ranging from 500 to 10 nM were injected over approximately 100 RUs of immobilized K4 and over a control dextran surface. The points correspond to the RUs obtained after double referencing. The solid lines represent the fit when integrating the curves simultaneously using a simple Langmuirian model. (B) Residuals corresponding to A. (C) Global fit of the E4 interaction with K4 using the conformational change (rearrangement) model. (D) Residuals from C.

fitting this interaction was found to be relatively fast ($k_{ass\#1} = 3.2 \times 10^6$ M^{-1} s^{-1}). The off-rate ($k_{diss\#1}$) was determined to be 2.0×10^{-4} s^{-1}, indicating that the coiled-coil complexes dissociate very slowly. Using these kinetic constants, we calculated the thermodynamic dissociation constant for the interaction ($K_d = k_{diss\#1}/k_{ass\#1} = 63$ pM). On-rates in the range of 10^6 M^{-1} s^{-1} have been found to be the upper limit for accurate determination using the BIACORE. With faster on-rates, the diffusion of the analyte from the bulk solution to the sensor chip surface may become rate limiting (*51*). To test for the presence of this mass transport limitation effect in our data, we fit the sensorgrams using a model depicting a simple peptide−peptide interaction coupled to a mass transport limitation. The kinetic constants determined with this model were found to be the same as those obtained with the simple model, within 5% error (data not shown). This demonstrates that our experimental conditions were adequate and that the results were not biased by mass transport/rebinding artifacts. The same approach was then applied to the other coiled-coil systems.

Surprisingly, global fitting of the data sets obtained for every other coiled-coil interaction (namely, E5/K4, E4/K5, E4/K4, E5/K3, and E4/K3) clearly showed deviations from a simple binding mechanism. This deviation was particularly noticeable during the wash-off phase (Figure 4A and 4B, and data not shown). Since artifacts that could lead to such a deviation were eliminated by optimizing experimental conditions, this deviation is likely due to a more complex biological mechanism of binding. We recently reported titrations of E4 into K4 (and vice versa) and showed that the maximum α-helical structure, as monitored by CD spectroscopy, occurred at 1:1 peptide ratios (*23*), confirming a 1:1 stoichiometry of E4 and K4 in the coiled-coil structure.

Previous reports stated that some coiled-coil dimers can undergo a conformational change (*52*). Additionally, other reports using sedimentation equilibrium experiments with the E4/K4 coiled-coil detected the presence of tetramers composed of two E and two K strands at high concentration (*23*). Accordingly, we used two more complex models to fit the data: the first one depicts a change in the conformation or a rearrangement of the E/K complex (the second kinetic step is first order, Figure 2B) ,while the second model represents the interaction of two E/K dimers to form a tetramer (the second kinetic step is second order, Figure 2C). The quality of the data fits was judged by the standard deviation of the residuals, and the Z1 and Z2 statistics. In all the cases (except the E3/K3 interaction; discussed below), the model best depicting the experimental data was the one representing a rearrangement of the coiled-coils (Table 2). The kinetic constants and the related thermodynamic dissociation constants calculated using this model are shown in Figure 5 and Table 3. To confirm that the dimer-to-tetramer model cannot account for the complex kinetic behavior, additional experiments were performed using C1 sensor chips (flat surface) rather than B1 sensor chips (long dextran chains). The rationale for this experimental approach is that the use of the C1 sensor chip should minimize the mobility of the coiled-coil complexes at the biosensor surface and inhibit tetramerization, if it was occurring. In the case of E4 being injected over immobilized K4, the rearrangement model was again found to best depict the interaction (data not shown), confirming the relevance of this model.

In the case of the E3/K3 interaction, due to the low affinity of binding, it was necessary to couple 1200 RUs of K3 to get an acceptable signal-to-noise ratio (30 RUs maximum). The three curves corresponding to the highest concentrations of E3 (40, 20, and 10 μM) were globally fit with the rearrangement model. The quality of the fit was relatively good, but the error for the off-rate of the second step was larger than the off-rate parameter value itself, thus indicating that the global fitting approach was not appropriate to analyze this set of data. Nevertheless, using the plateau value of these

Table 2: Standard Deviation (S.D.) of the Residuals and Z1 and Z2 Statistics Calculated When Applying a Simple, a Conformational Change (rearrangement), or a Dimer−Tetramer Model to Globally Fit the Sensorgrams for the Different Coiled-Coil Interactions[a]

		E/K coil interactions					
		E5/K5	E4/K5	E5/K4	E4/K4	E5/K3	E4/K3
S.D.	Simple	**1.07**	1.32	1.50	2.43	1.79	2.07
	Rearrangement	1.07	**1.03**	**1.20**	**1.28**	**1.01**	**0.94**
	Dimer-to-tetramer	1.07	1.24	1.33	1.44	1.10	1.00
Z1	Simple	**7.79**	15.72	26.26	35.75	19.56	28.59
	Rearrangement	7.79	**7.89**	**15.30**	**18.37**	**8.85**	**18.13**
	Dimer-to-tetramer	7.79	14.28	19.93	19.40	13.21	18.53
Z2	Simple	**0.75**	0.194	1.63	1.56	1.71	2.61
	Rearrangement	0.75	**0.147**	**0.83**	**0.72**	**0.59**	**1.28**
	Dimer-to-tetramer	0.75	0.379	0.85	0.75	0.71	1.47

[a] Low scores are indicative of good fits, and the best scores are in bold print.

three curves, we determined an apparent K_d value of 32 μM by Scatchard analysis for the E3/K3 interaction.

Using the kinetic constants determined from the rearrangement model (Table 3) for all the E/K coiled-coil interactions (except E5/K5), we simulated the time-dependent variation of the initial and rearranged EK complexes at a set E coil concentration and a set amount of immobilized K coil. Figure 6 shows the simulation of the injection of 500 nM of E4 over a surface amount of K4 that is the same as that shown in Figure 4. The plot shows that, at the end of the injection, the amount of initial and rearranged complexes were essentially equal. Lipschultz et al. introduced the concept that association times that achieve T_{50} (the time at which the amount of initial and rearranged complex are equal) should be used to confirm the existence or absence of a complex kinetic mechanism (*53*). Our simulation confirmed that the experimental conditions that we used in the case of E4/K4 allowed T_{50} to be reached. The same type of simulation was also performed for the other coiled-coil interactions and indicated that the injection times and concentrations used resulted in T_{50} being achieved (data not shown).

DISCUSSION

To study the interactions of the different length E and K coils using the BIACORE, we coupled the K coils via a disulfide bond to the sensor chip surfaces. This immobilization approach, combined with optimization of experimental conditions, enabled us to eliminate artifacts (surface heterogeneity, parking problems, and mass transport limitations) that could have biased subsequent data analysis.

The interaction of E5 and K5, the longest peptides used in this study, was well described by a simple mechanism where the unfolded monomeric peptides are converted to the fully folded dimer without discernible intermediates. The remarkably high affinity (K_d = 63 pM) agrees with previous results using urea and guanidine-HCl denaturations, as monitored by circular dichroism spectroscopy (*22*). This stability results from the combination of hydrophobic interactions (involving the residues at positions a and d of each heptad) and electrostatic interactions (positions e and g) between the two de novo designed α-helices and is reflected in a relatively fast association, or on-rate, of the two peptides ($k_{ass\#1} = 3.2 \times 10^6$ M^{-1} s^{-1}) and a very slow dissociation, or off-rate, of the coiled-coil ($k_{diss\#1} = 2.0 \times 10^{-4}$ s^{-1}). This off-rate is in good agreement with previous BIACORE experiments conducted by Chao et al. (*22*), who found a $k_{diss\#1}$ value of 2.1×10^{-4} s^{-1} when injecting a streptavidin-bound biotinylated E5 coil over K5. The on-rate ($k_{ass\#1} = 4.5 \times 10^5$ M^{-1} s^{-1}) is 10 fold lower than ours, which is likely due to the fact that the analyte E5 coil was linked to streptavidin. This suggests that the attachment of a protein at the C terminus of the E5 coil influenced only the on-rate of binding, without affecting the dissociation rate, hence the stability, of the dimer.

The E5/K5 heterodimer is among the most stable of the de novo designed coiled-coils that have been studied. Wendt et al. (*54*) examined the interaction of the de novo designed A/B heterodimeric coiled-coil by stopped-flow fluorescence. This system displayed a rapid, ionic strength-dependent association rate ($k_{ass} = 3.7-72 \times 10^6$ M^{-1} s^{-1}) that is in the same range as the one that we observed for E5/K5.

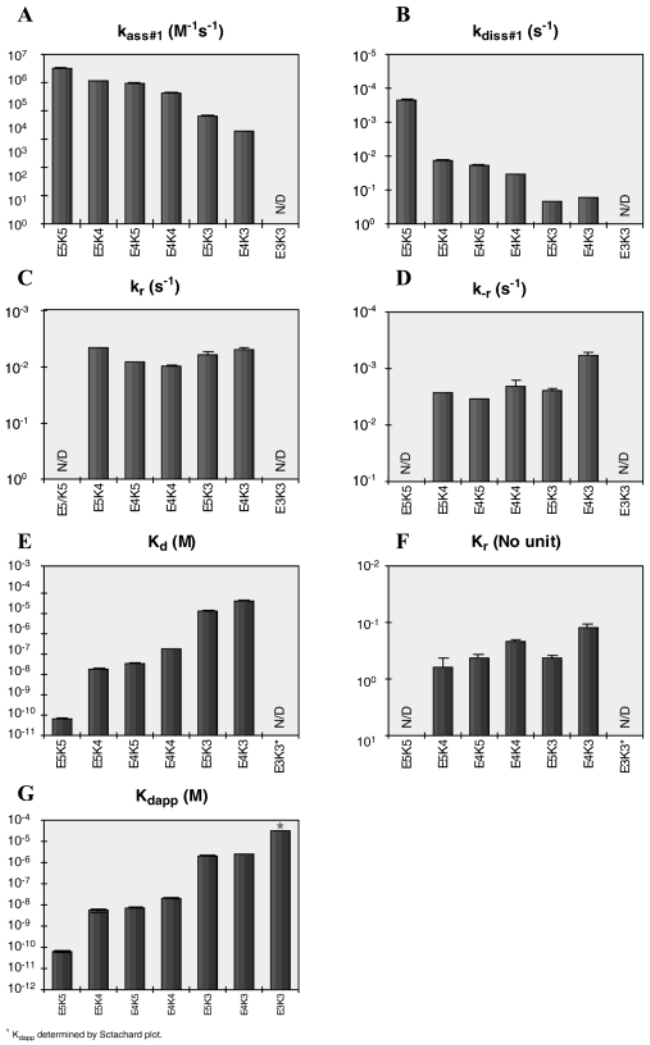

FIGURE 5: The effect of chain length on the kinetic and thermodynamic constants for the E/K interactions derived when using the conformational change (rearrangement) model. Panels A to D: $k_{ass\#1}$, $k_{diss\#1}$, k_r, and k_{-r} kinetic constants, as determined by globally fitting the different coiled-coil interactions with the conformational change model. Panels E to G: The K_d, K_r, and K_{dapp} thermodynamic constants that were calculated using the kinetic constants. *K_{dapp} was determined by Scatchard plot.

Interestingly, the dissociation rates that they observed (k_{diss} = 3.8−10 × 10^2 s^{-1}), which are considerably faster than ours, were independent of ionic strength. This emphasizes the important role that electrostatic interactions can play in heterodimer association. An even faster association rate (k_{ass} = 10^7−10^8 M^{-1} s^{-1}) was measured for the acidic peptide A at pH 3.0 or at very high ionic strength (*55*, *56*); however, these conditions are far from physiological. Extensive studies of the folding of GCN4-p1 have yielded association constants in the range of 10^5−10^6 M^{-1} s^{-1}, which are closer to the ones that we observed for E5/K5 (*57*−*59*). These variations can be explained by small sequence changes, or differences in the techniques (e.g., presence of fluorescent labels) or the solvent conditions.

Somewhat surprisingly, we found that the interaction of the coiled-coils of every combination of chain length other than E5/K5 did not fit the simple Langmuirian model (Figure 4A,B and data not shown). We tested two mechanistic models to see if we could account for these more complex interaction kinetics: one, a rate limiting rearrangement of the complex after the initial binding event, and, two, the formation of a tetramer after dimerization (Figure 2). We chose the first model because a conformational change was previously reported for a coiled-coil system (*52*). We chose the second model since sedimentation equilibrium experiments have shown that E5/K5 can form a tetramer with a dissociation constant ($K_{d\ dimer-tetramer}$) equal to 200 μM (*22*). Additionally, the observed molecular weight in sedimentation equilibrium experiments of E4/K4 was midway between that of the dimeric and tetrameric species, indicative of a dimer−tetramer equilibrium at high concentrations (*23*). An interaction between two EK dimers within the matrix of the biosensor is theoretically possible since the dextran chains have been shown to be flexible enough to allow for such an interaction (*60*). However, it is unlikely that tetramerization accounts for the complex kinetics that we have observed since our global analysis of the experimental data showed that all coiled-coil interactions, except for E5/K5, were best described by a model that includes a rearrangement of the EK dimer. Furthermore, the use of C1 sensor chips, which would inhibit tetramerization on the surface, did not result in a simplification of the E4/K4 interaction data. The high quality of the fit for the rearrangement model is illustrated by the random character of the residuals (Figure 4), and the low values for the standard deviation of the residuals and the Z1 and Z2 statistics (Table 2). It should be stated, however, that we cannot exclude the possibility that a complex with a stoichiometry greater than one-to-one may occur at the biosensor surface, and that this could affect the data analysis.

In support of the rearrangement model, biphasic interaction mechanisms have previously been observed for coiled-coils. Although monophasic folding has been observed for GCN4-p1 and related peptides by a number of researchers, using techniques such as DSC, stopped-flow CD and fluorescence spectroscopy (*54*, *57*−*59*), biphasic folding has been reported by others using stopped-flow fluorescence experiments with GCN4-p1 (*61*, *62*) and analogues of the de novo designed LZ peptides (*53*). Additionally, Holtzer and co-workers have conducted extensive $^{13}C^{\alpha}$ NMR experiments in which the transition of a coiled-coil from the unfolded to the folded state is monitored at specific residues (*63*−*67*). This work provided persuasive evidence that these coiled-coil dimers exist in at least two distinct folded states.

A few researchers have observed a switch from monophasic to biphasic interaction mechanisms upon relatively minor sequence changes. Holtzer and co-workers found that the peptides GCN4-lz and GCN4-lzK, which differ by four conservative mutations (Arg to Lys and His to Lys), folded by monophasic and biphasic mechanisms, respectively (*66*). Mutational ϕ analysis by Moran et al. (*68*) found that oxidation of the peptide GCN4-p2 (which has an N-terminal CGG extension) appeared to restrict folding to a single transition state as compared to the multiple transition states available to the reduced peptide.

Wendt and co-workers showed by stopped-flow fluorescence that the de novo designed LZ, LZ(12A), or LZ(16A) coiled-coils obeyed complex kinetics of dissociation that could be depicted, as in our case, by the presence of a change in the conformation of the dimer (*52*). Additionally, Zhu et al. (*62*) recently showed that the thermal unfolding of a GCN4 variant in which the Asn residue was moved from

Table 3: Kinetic and Thermodynamic Constants Related to the Global Fit of Interactions of the Different E/K Coiled-Coil Pairs When Using a Conformational Change (Rearrangement) Model[a]

parameter (unit)	E/K coiled-coils ± value 95% confidence interval)						
	E5/K5	E5/K4	E4/K5	E4/K4	E5/K3	E4/K3	E3/K3
$k_{ass\#1}$ ($M^{-1}s^{-1}$)	$(3.17 \pm 0.05) \times 10^6$	$(9.2 \pm 0.2) \times 10^5$	$(7.3 \pm 0.2) \times 10^5$	$(2.89 \pm 0.07) \times 10^5$	$(3.1 \pm 0.2) \times 10^4$	$(7.3 \pm 0.4) \times 10^3$	n/d
$k_{diss\#1}$ (s^{-1})	$(2.0 \pm 0.1) \times 10^{-4}$	$(1.29 \pm 0.08) \times 10^{-2}$	$(1.8 \pm 0.2) \times 10^{-2}$	$(3.4 \pm 0.2) \times 10^{-2}$	$(2.2 \pm 0.1) \times 10^{-1}$	$(1.67 \pm 0.06) \times 10^{-1}$	n/d
k_r (s^{-1})	n/a	$(4.4 \pm 0.6) \times 10^{-3}$	$(8.0 \pm 0.7) \times 10^{-3}$	$(9.6 \pm 0.3) \times 10^{-3}$	$(5.83 \pm 0.2) \times 10^{-3}$	$(4.8 \pm 0.2) \times 10^{-3}$	n/d
k_{-r} (s^{-1})	n/a	$(2.7 \pm 0.4) \times 10^{-3}$	$(3.4 \pm 0.2) \times 10^{-3}$	$(2.10 \pm 0.09) \times 10^{-3}$	$(2.5 \pm 0.1) \times 10^{-3}$	$(5.9 \pm 0.5) \times 10^{-4}$	n/d
K_d (M)	$(6.3 \pm 0.5) \times 10^{-11}$	$(1.4 \pm 0.1) \times 10^{-8}$	$(2.5 \pm 0.2) \times 10^{-8}$	$(1.16 \pm 0.08) \times 10^{-7}$	$(7.0 \pm 0.8) \times 10^{-6}$	$(2.3 \pm 0.2) \times 10^{-5}$	n/d
K_r (no unit)	n/a	0.6 ± 0.2	(0.42 ± 0.06)	(0.22 ± 0.02)	(0.42 ± 0.04)	(0.12 ± 0.01)	n/d
K_{dapp} (M)	$(6.3 \pm 0.5) \times 10^{-11}$	$(5.4 \pm 1) \times 10^{-9}$	$(7.3 \pm 0.4) \times 10^{-9}$	$(2.08 \pm 0.03) \times 10^{-8}$	$(2.11 \pm 0.08) \times 10^{-6}$	$(2.51 \pm 0.04) \times 10^{-6}$	$(3.2 \pm 0.3) \times 10^{-5}$*

[a] n/a: not applicable; n/d: not determined; *determined by Scatchard analysis (3 independent experiments).

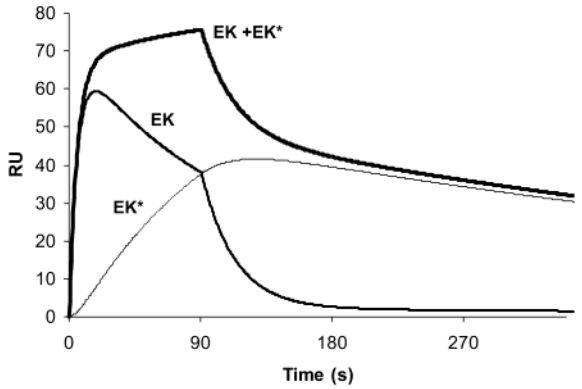

FIGURE 6: Simulation of the time-dependent variation of the E4/K4 complexes. The simulation was done with the same Runge−Kutta algorithm as in SP*Revolution* and the parameters for the rearrangement model as listed in Table 3. The concentration of injected E4 was set at 500 nM and the K4 quantity as 90 RU. The sum of the initial (EK) and rearranged (EK∗) complex corresponds to the RU signal (EK + EK∗) that was recorded for the highest concentration shown in Figure 4A.

position 16 to 9 followed a multi-state transition mechanism. The authors were able to show the presence of a transient, partially folded intermediate. Since these coiled-coil systems have an Asn residue at a central a position, alternative alignments are destabilized, i.e., out-of-register binding in which not all the heptads are interacting is unfavorable. Accordingly, it is likely that the presence of aligned and unaligned species cannot account for the complex kinetics of dissociation that were observed in these cases and in the present study.

Together, these results strongly suggest that the first-order kinetic rearrangement of the coiled-coils that we report here may be a common phenomenon. Since the forward rates for the rearrangement for the E/K dimers were in the range of 10^{-3} s^{-1} (Figure 5C), and were relatively independent of the length of the coils, such a change in the conformation could also occur for the E5/K5 pair without being kinetically limiting, and hence be undetectable.

The kinetic constants (Figure 5A−D) indicate that the monomer−dimer association and dissociation steps are the most sensitive to variations in chain length. The on-rates ($k_{ass\#1}$) vary from 10^4 (E4/K3) to 3.2×10^6 M^{-1} s^{-1} (E5/K5) in an exponential fashion. Interestingly, the off-rates ($k_{diss\#1}$) appear to be dependent on the length of the shortest coil of an E/K pair; $k_{diss\#1}$ is in the range of 10^{-1}, 10^{-2}, and 10^{-4} s^{-1} when the shortest coil is composed of three, four, or five heptads, respectively. This results in a large variation in the first equilibrium constant (K_d, Figure 5E), which ranges from 100 pM to 10 μM, as the length of the shortest coil varies from five to three heptads. As stated above, the kinetic constants related to the second step (rearrangement) do not markedly vary with the lengths of the coils (a less than 10-fold difference is observed for k_r and k_{-r}). This results in a relatively small variation (from 0.1 to 1) in the second equilibrium constant (K_r, Figure 5F). From both K_d and K_r, it is possible to calculate an apparent dissociation constant K_{dapp} (Figure 5G) which takes into account both rearranged and unrearranged E/K dimers at equilibrium. For example, the E4/K4 heterodimer was found to have an apparent K_d equal to 1.2×10^{-7} M. The equation $\Delta G = RT \ln K_{dapp}$ was used to calculate the free energy of association as −9.4 kcal/mol. This is in fairly good agreement with the free energy obtained by linear extrapolation analysis of a GdnHCl denaturation curve for the same molecule (−8.2 kcal/mol, see ref *23*), especially considering that these two techniques are based on different principles and assumptions.

Increases in chain length have been clearly shown to cause increases in stability, though in a nonlinear relationship (*23*, *69*, *70*). One obvious stabilizing effect of increased chain length is the increase in the number of stabilizing contacts, such as hydrophobic interactions at the coiled-coil interface and e to g′ electrostatic attractions. Recent studies have shown that valine at a central a position contributes 1.66 kcal/mol more than alanine, and leucine at a central d position contributes 3.8 kcal/mol more than alanine (*35*, *36*). The other key factor is end fraying, a partial and temporary unfolding of the helix termini. In the case of the recent study carried out by Zhu et al. (*62*), the observed rearrangement of the dimeric coil was attributed to an increase in the fraying of the N-terminal ends of the coils which was induced by an Asn mutation. This fraying phenomenon may also account at least partially, if not totally, for the rearrangement step that we have observed.

Indeed, such a fraying phenomenon has been previously reported for dimeric de novo designed coiled-coils. Specifically, Zhou et al. (*37*) observed only a small decrease in

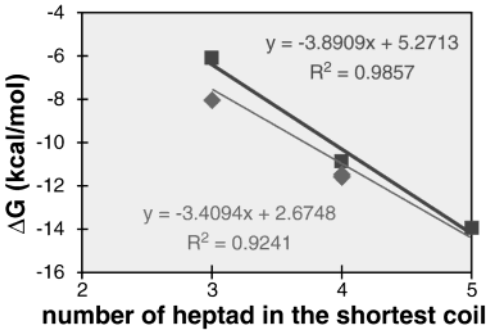

FIGURE 7: Variation of the free energy of binding with the length of the shortest coil within the dimers. The thick line and top equation correspond to the linear regression when taking into account the length-matched coil pairs (E3/K3, E4/K4, and E5/K5; square dots) and the thin line and bottom equation to linear regression when taking into account all the coiled-coil interactions (all dots).

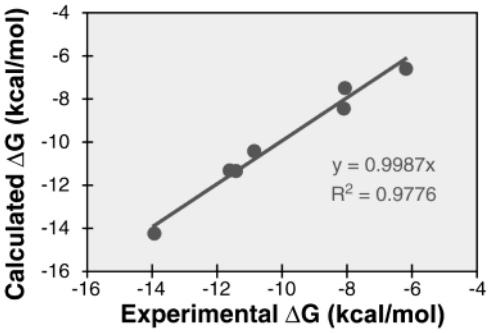

FIGURE 8: Experimental free energies versus free energies calculated using the multiple-linear regression approach.

stability at either end of a de novo designed parallel coiled-coil, when systematically performing Leu−Ala substitution at every a and d positions of a 35-residue polypeptide chain. This demonstrated that the contribution of Leu−Leu hydrophobic interactions to the stability of the coiled-coil structure were less important at the ends of the coiled-coil, and that the ends of the coiled-coil were more flexible. More recently, Holtzer et al. (*65*) clearly demonstrated by $^{13}C^{\alpha}$ chemical shifts that such an end-fraying also occurred in a GCN4-like leucine zipper. All these studies suggest that the different heptads which make up a dimeric coiled-coil structure contribute differently to its stability; the heptads located at the ends of the coiled-coil are able to fray whereas the ones composing the core of the coiled-coil are more stable due to the tighter packing of the hydrophobic residues.

From the apparent K_d shown in Figure 5G, it appears that the main factor governing the overall stability of the dimer is the length of the shortest coil present in the complex. This conclusion is even more obvious when plotting the free energy (ΔG), deduced from the K_{dapp} as a function of the length of the shortest coil involved in the dimers (Figure 7). The contribution of the heptads which are not in direct contact with the other strand is minimal as compared to the ΔG contribution of the paired ones, since there is only a 15% change in the slope of the regression lines depending on whether the ΔG corresponding to the mismatching length coiled-coil interactions are taken into account during the regression or not.

From the linear equation corresponding to the matching pairs of E/K (Figure 7), it is possible to deduce the ΔG contribution of the heptads composing the core of the coiled-coil (ΔG_{core}) versus the ΔG contribution of the heptads at the ends of the dimers ($\Delta G_{paired-end}$). That is, the slope of the curve corresponds to the contribution of a heptad composing the core and is equal to −3.89 kcal/mol of dimerized core heptad; $\Delta G_{paired-end}$ can be obtained by term substitution, giving a value of −1.26 kcal/mol per heptad involved in the paired-end.

In an effort to refine the calculations and take the mismatching length coiled-coil interactions into consideration, we assigned to the heptads composing the dimers one of the three following ΔG values, depending if the heptad is part of the core (ΔG_{core}), part of one of the two paired-ends ($\Delta G_{paired-end}$), or is not in direct contact with the other strand ($\Delta G_{unpaired-end}$). This corresponds to defining a system of seven equations (one for each coiled-coil interaction studied) that can be solved by multiple-linear regression. Figure 8 shows the results of such an approach and gives a ΔG_{core} value of −3.84, a $\Delta G_{paired-end}$ value of −1.38 and a $\Delta G_{unpaired-end}$ value of −0.93 kcal/mol of heptads with a R^2 coefficient of 0.9776. The two approaches to calculating the ΔG contribution of a heptad give remarkably close estimations for the ΔG contribution of the heptads composing the core versus the ends of the coiled-coil and clearly indicate that the ΔG contribution of the core heptads is 3-fold higher than the ΔG contribution of the heptads located at the ends of the dimer. These differences in the contribution of the core versus the end heptads to the stability of the dimer are consistent with our E3/K3 data which demonstrated that this interaction is low affinity, i.e., such a low affinity can be attributed to the presence of only one core heptad in the coiled-coil dimer. Similarly, Su et al. (*70*) showed, by varying the length of a coil whose heptad motif was IEALKAE, that a minimum of three heptads was required to form a stable two-stranded α-helical coiled-coil.

In conclusion, we have shown that the association of heterodimeric coiled-coils can be studied with the BIACORE. The E5/K5 interaction was found to be rapid and of high affinity, and could be described by a simple mechanism. The shorter E/K coiled-coil interactions were better depicted by a more complex mechanism, i.e., dimer formation followed by a conformational rearrangement. Analysis of the relationship between affinity and chain length suggested that heptads at different positions within the coiled-coil provide different amounts of free energy. Specifically, the core heptads contributed more than twice as much to the free energy of interaction as compared to heptads at the ends of the coiled-coil. As expected, heptads at the ends that were paired (i.e., the two strands were of the same length) contributed more than unpaired heptads. However, unpaired heptads did contribute slightly to the free energy of binding, giving mismatched coiled-coils an intermediate stability, with respect to the two matched pairs.

The generation of a series of E/K heterodimeric coiled-coils with varying length and, consequently, a wide range of stabilities and affinities provides for considerable flexibility in designing applications based on these coiled-coils. For instance, a single protein (e.g., an E5-fusion) could be used in several applications that require different degrees of coiled-coil stability, e.g., purification versus immobilization, by simply varying the length of the partner K coil.

ACKNOWLEDGMENT

The authors want to acknowledge Drs. Sulea and Lortie at the Biotechnology Research Institute for fruitful discussion during the writing of this manuscript.

REFERENCES

1. Burkhard, P., Stetefeld, J., and Strelkov, S. V. (2001) *Trends Cell Biol. 11*, 82−88.
2. Kohn, W. D., Mant, C. T., and Hodges, R. S. (1997) *J. Biol. Chem. 272*, 2583−2586.
3. Lupas, A. (1996) *Trends Biochem. Sci. 21*, 375−382.
4. Muller, K. M., Arndt, K. M., and Alber, T. (2000) *Methods Enzymol. 328*, 261−282.
5. Kohn, W. D., and Hodges, R. S. (1998) *Trends Biotechnol. 16*, 379−389.
6. Crick, F. H. C. (1953) *Acta Crystallogr. 6*, 689−697.
7. Krylov, D., Mikhailenko, I., and Vinson, C. (1994) *EMBO J. 13*, 2849−2861.
8. Lavigne, P., Kondejewski, L. H., Houston, M. E., Jr., Sonnichsen, F. D., Lix, B., Skyes, B. D., Hodges, R. S., and Kay, C. M. (1995) *J. Mol. Biol. 254*, 505−520.
9. Vinson, C. R., Hai, T., and Boyd, S. M. (1993) *Genes Dev. 7*, 1047−1058.
10. Kohn, W. D., Kay, C. M., and Hodges, R. S. (1995) *Protein Sci. 4*, 237−250.
11. Kohn, W. D., Monera, O. D., Kay, C. M., and Hodges, R. S. (1995) *J. Biol. Chem. 270*, 25495−25506.
12. Kohn, W. D., Kay, C. M., and Hodges, R. S. (1998) *J. Mol. Biol. 283*, 993−1012.
13. Graddis, T. J., Myszka, D. G., and Chaiken, I. M. (1993) *Biochemistry 32*, 12664−12671.
14. Katz, B. Z., Krylov, D., Aota, S., Olive, M., Vinson, C., and Yamada, K. M. (1998) *Biotechniques 25*, 298−302, 304.
15. Myszka, D. G., and Chaiken, I. M. (1994) *Biochemistry 33*, 2363−2372.
16. Zhou, N. E., Kay, C. M., and Hodges, R. S. (1994) *J. Mol. Biol. 237*, 500−512.
17. O'Shea, E. K., Rutkowski, R., and Kim, P. S. (1992) *Cell 68*, 699−708.
18. Rieker, J. D., and Hu, J. C. (2000) *Methods Enzymol. 328*, 282−296.
19. Chao, H., Bautista, D. L., Litowski, J., Irvin, R. T., and Hodges, R. S. (1998) *J. Chromatogr. B Biomed. Sci. Appl. 715*, 307−329.
20. Hodges, R. S. (1996) *Biochem. Cell Biol. 74*, 133−154.
21. Tripet, B., Yu, L., Bautista, D. L., Wong, W. Y., Irvin, R. T., and Hodges, R. S. (1996) *Protein Eng. 9*, 1029−1042.
22. Chao, H., Houston, M. E., Jr., Grothe, S., Kay, C. M., O'Connor-McCourt, M., Irvin, R. T., and Hodges, R. S. (1996) *Biochemistry 35*, 12175−12185.
23. Litowski, J. R., and Hodges, R. S. (2001) *J. Pept. Res. 58*, 477−492.
24. Litowski, J. R., and Hodges, R. S. (2002) *J. Biol. Chem.*, in press.
25. Rich, R. L., and Myszka, D. G. (2000) *Curr. Opin. Biotechnol. 11*, 54−61.
26. Erickson, B. W., and Merrifield, R. B. (1976) "Solid-Phase Peptide Synthesis" in *The Proteins*, Vol. II, 3rd ed. (Neurath, H., Hill, R. L., and Boeder, C.-L., Eds.) pp 255−527, Academic Press, New York.
27. Sereda, T. J., Mant, C. T., Quinn, A. M., and Hodges, R. S. (1993) *J. Chromatogr. 646*, 17−30.
28. Fivash, M., Towler, E. M., and Fisher, R. J. (1998) *Curr. Opin. Biotechnol. 9*, 97−101.
29. O'Connor-McCourt, M. D., De Crescenzo, G., Lortie, R., Lenferink, A. E. G., and Grothe, S. (1998) in *Quantitative Analysis of Biospecific Interactions* (Lundqvist, A. and Greijer, E., Eds.) pp 175−190, Harwood Academic Publisher, GMBH, Chur, Switzerland.
30. De Crescenzo, G., Grothe, S., Lortie, R., Debanne, M. T., and O'Connor-McCourt, M. (2000) *Biochemistry 39*, 9466−9476.
31. Press, W. H., Flannery, B. P., Teukolsky, S. A., and Vetterling, W. T. (1986) *Numerical Recipes, The Art of Scientific Computing*, Cambridge University Press, Cambridge.
32. Marquardt, D. W. (1963) *J. Soc. Indust. Appl. Math. 11*, 431−441.
33. Bradley, J. V. (1968) *Distribution-Free Statistical Tests*, Prentice-Hall, Englewood, NJ.
34. Harbury, P. B., Zhang, T., Kim, P. S., and Alber, T. (1993) *Science 262*, 1401−1407.
35. Tripet, B., Wagschal, K., Lavigne, P., Mant, C. T., and Hodges, R. S. (2000) *J. Mol. Biol. 300*, 377−402.
36. Wagschal, K., Tripet, B., Lavigne, P., Mant, C., and Hodges, R. S. (1999) *Protein Sci. 8*, 2312−2329.
37. Zhou, N. E., Kay, C. M., and Hodges, R. S. (1992) *Biochemistry 31*, 5739−5746.
38. Chakrabartty, A., Kortemme, T., and Baldwin, R. L. (1994) *Protein Sci. 3*, 843−852.
39. Lyu, P. C., Liff, M. I., Marky, L. A., and Kallenbach, N. R. (1990) *Science 250*, 669−673.
40. Monera, O. D., Sereda, T. J., Zhou, N. E., Kay, C. M., and Hodges, R. S. (1995) *J. Pept. Sci. 1*, 319−329.
41. O'Neil, K. T., and DeGrado, W. F. (1990) *Science 250*, 646−651.
42. Moitra, J., Szilak, L., Krylov, D., and Vinson, C. (1997) *Biochemistry 36*, 12567−12573.
43. Zhu, B. Y., Zhou, N. E., Kay, C. M., and Hodges, R. S. (1993) *Protein Sci. 2*, 383−394.
44. Fisher, R. J., and Fivash, M. (1994) *Curr. Opin. Biotechnol. 5*, 389−395.
45. Morton, T. A., Myszka, D. G., and Chaiken, I. M. (1995) *Anal. Biochem. 227*, 176−185.
46. Karlsson, R., and Falt, A. (1997) *J. Immunol. Methods 200*, 121−133.
47. Kortt, A. A., Oddie, G. W., Iliades, P., Gruen, L. C., and Hudson, P. J. (1997) *Anal. Biochem. 253*, 103−111.
48. O'Shannessy, D. J., and Winzor, D. J. (1996) *Anal. Biochem. 236*, 275−283.
49. Myszka, D. G., Morton, T. A., Doyle, M. L., and Chaiken, I. M. (1997) *Biophys. Chem. 64*, 127−137.
50. Myszka, D. G. (1999) *J. Mol. Recognit. 12*, 279−284.
51. Myszka, D. G. (1997) *Curr. Opin. Biotechnol. 8*, 50−57.
52. Wendt, H., Berger, C., Baici, A., Thomas, R. M., and Bosshard, H. R. (1995) *Biochemistry 34*, 4097−4107.
53. Lipschultz, C. A., Li, Y., and Smith-Gill, S. (2000) *Methods 20*, 310−318.
54. Wendt, H., Leder, L., Harma, H., Jelesarov, I., Baici, A., and Bosshard, H. R. (1997) *Biochemistry 36*, 204−213.
55. Durr, E., Jelesarov, I., and Bosshard, H. R. (1999) *Biochemistry 38*, 870−880.
56. Jelesarov, I., Durr, E., Thomas, R. M., and Bosshard, H. R. (1998) *Biochemistry 37*, 7539−7550.
57. Ibarra-Molero, B., Makhatadze, G. I., and Matthews, C. R. (2001) *Biochemistry 40*, 719−731.
58. Sosnick, T. R., Jackson, S., Wilk, R. R., Englander, S. W., and DeGrado, W. F. (1996) *Proteins 24*, 427−432.
59. Zitzewitz, J. A., Bilsel, O., Luo, J., Jones, B. E., and Matthews, C. R. (1995) *Biochemistry 34*, 12812−12819.
60. Myszka, D. G., Arulanantham, P. R., Sana, T., Wu, Z., Morton, T. A., and Ciardelli, T. L. (1996) *Protein Sci. 5*, 2468−2478.
61. Wendt, H., Baici, A., and Bosshard, H. R. (1994) *J. Am. Chem. Soc. 116*, 6973−6974.
62. Zhu, H., Celinski, S. A., Scholtz, J. M., and Hu, J. C. (2001) *Protein Sci. 10*, 24−33.
63. d'Avignon, D. A., Bretthorst, G. L., Holtzer, M. E., and Holtzer, A. (1998) *Biophys. J. 74*, 3190−3197.
64. d'Avignon, D. A., Bretthorst, G. L., Holtzer, M. E., and Holtzer, A. (1999) *Biophys. J. 76*, 2752−2759.
65. Holtzer, M. E., Lovett, E. G., d'Avignon, D. A., and Holtzer, A. (1997) *Biophys. J. 73*, 1031−1041.
66. Holtzer, M. E., Bretthorst, G. L., d'Avignon, D. A., Angeletti, R. H., Mints, L., and Holtzer, A. (2001) *Biophys. J. 80*, 939−951.
67. Lovett, E. G., d'vignon, D. A., Holtzer, M. E., Braswell, E. H., Zhu, D., and Holtzer, A. (1996) *Proc. Natl. Acad. Sci. U.S.A. 93*, 1781−1785.
68. Moran, L. B., Schneider, J. P., Kentsis, A., Reddy, G. A., and Sosnick, T. R. (1999) *Proc. Natl. Acad. Sci. U.S.A. 96*, 10699−10704.
69. Lau, S. Y., Taneja, A. K., and Hodges, R. S. (1984) *J. Biol. Chem. 259*, 13253−13261.
70. Su, J. Y., Hodges, R. S., and Kay, C. M. (1994) *Biochemistry 33*, 15501−15510.

BI0268450